Modelling the Dynamic Viscous and Thermal Dissipation Mechanisms in a Fibrous Porous Material

B.P. Semeniuk[1], and P. Göransson[1]
[1]KTH Royal Institute of Technology, Department of Aeronautical & Vehicle Engineering
100 44 Stockholm, Sweden, semeniuk@kth.se

Abstract

The main mechanisms of acoustic attenuation in lightweight fibrous porous materials are the dynamic viscous drag forces on the surface of the fibres, and the thermal heat transfer between the solid fibres and the surrounding fluid. Microstructure models have been recently developed which consider these micro-level interactions analytically [1], allowing the simulation of coupled acoustic and structural wave propagation through the three-dimensional, highly porous acoustic thermal insulation material using only the geometrical fibre properties, the constitutive properties of the solid fibre material and surrounding fluid, and the macroscopic elastic properties. A key assumption in this approach is that the fibre spacing is large enough such that the viscous and thermal dissipation fields surrounding the fibres should not significantly interact. In support of this new poroelastic model development, the thermoviscous acoustic fluid analysis capabilities of COMSOL have been utilized as a *virtual laboratory*, in order to assess the interaction of the coupled viscous and thermal boundary layers on a representative array of cylindrical fibres.

Introduction

Recent work into the characterisation of fibrous porous materials has strongly focussed on microstructural aspects, i.e. the fibre diameter distributions, fibre orientation angles, and the distributions of fibre lengths [2, 3] in order to predict the transport properties of the material. In practice, this means that a combination of numerical and experimental techniques are used to estimate the macroscopic transport properties of the fibrous material, such as static viscous and thermal permeabilities, viscous characteristic lengths, and high frequency tortuosity. Using this information, the vibroacoustic performance may then be simulated using established Biot-based poroelastic models [4], for example. Unfortunately, this approach often requires the assumption of an approximated pore structure, and either complex fluid flow and thermal diffusion simulations, existing material samples for laboratory measurements, or additional steps in order to predict acoustic performance.

It would be much more convenient if the microstructural aspects of the fibrous material were taken into account analytically in the formulation of the governing poroelastic equations, meaning direct relationships between physical properties such as fibre diameter distributions and orientation angles, and resulting acoustic performance could be made in an efficient way.

To address this, we have re-approached the problem at a fundamental level, intentionally independent from existing poroelastic theories. Firstly, by considering the fibrous insulation material as a control volume of infinite solid cylindrical fibres embedded within an infinite viscous fluid, the resulting force balance allows us to derive the governing solid and fluid momentum equations in terms of viscous drag forces arising from the relative motion between the solid and fluid phases. Secondly, we have considered that when waves propagate through the porous fibrous material, oscillatory heat flow between the thermal fields of the solid fibres and the surrounding viscous fluid results in a corresponding non-equilibrium thermal expansion of the fluid. This then leads to a set of modified stress-strain relations for the coupled solid and fluid phases, and of a scaled fluid dilatation term representing the non-equilibrium heat transfer effects.

Fibre surface roughness and bonding between fibres are not considered in the viscous analysis. Viscous and thermal field interactions between neighbouring fibres are also neglected in the analytical expressions for viscous drag forces on the surface of the cylindrical fibres, and the heat transfer between the fibres and the surrounding viscous fluid. This means that the formulation is targeted at higher porosity materials having large spacings between fibres.

A transfer matrix (TM) formulation of the resulting governing equations has allowed a comparison against impedance tube acoustic absorption coefficient measurements for a rigidly-backed finite material sample. The initial simulation results have proven to be very promising. Subsequent thermoviscous acoustic fluid finite element modelling in COMSOL has allowed us to then fundamentally investigate the viscous and thermal

boundary layer interaction within a regular array of fibres as a means of better understanding dominant physical mechanisms, and confirming the underlying assumptions in the model, i.e. that there is not significant interaction between the viscous and thermal boundary layers of neighbouring fibres.

Material Definition

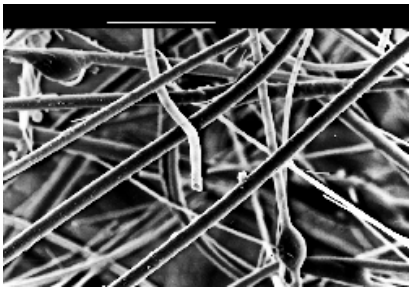

Figure 1. SEM micrograph of Johns Manville Microlite AA glass fibre thermal insulation material. 20 micrometre scaling.

The porous material used for this development is a lightweight (10 kg/m^3 bulk density), and flexible aircraft fuselage acoustical and thermal insulation from the Johns Manville Company, as shown in Figure 1. The solid fibre skeleton consists of a distribution of cylindrical glass fibres, having diameters ranging from 0.125 to 5.0 micrometres, with a mean fibre diameter of 1.28 micrometres, and standard deviation of 0.92 micrometres.

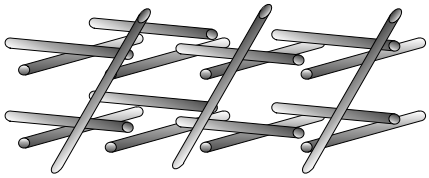

Figure 2. Transversely isotropic fibre representation.

The orientation of the fibres is assumed to be primarily transversely isotropic, with some fibres being orientated through the thickness of the material to provide structural integrity and compressional stiffness, as shown in Figure 2. A full description of the material, its microstructural, constitutive and elastic properties is provided in [1, 5].

Microstructure Derived Poroelastic Equation Summary

The governing coupled fluid-solid equations for this fibrous material are formulated using the assumption that the volume fraction is uniform throughout the solid, interconnected fibre skeleton; every plane cuts through a fraction ϕ of solid fibre per unit total area. It is also assumed that we do not have any pressure gradient forces at the fluid-fibre interfaces inside the control volume boundary. If the contents of the control volume are held constant, pressurising the fluid applies a compressive stress or dilatation of the solid fibre. Alternatively, if the control volume is held constant, applying a stress to the solid applies a pressure stress or dilatation to the fluid. This coupling between the solid fibres and surrounding fluid results in a set of stress-strain relations for the porous composite, which we assume to be transversely isotropic for the fibrous insulation material considered here.

Momentum Equations

Summarising the detailed formulation presented in [1], the equation of motion of the solid fibre skeleton (solid momentum equation) is written as

$$\phi\rho_s\ddot{u}_i = \left(\frac{\partial\sigma_{ii}}{\partial x_i}+\frac{\partial\sigma_{ij}}{\partial x_j}+\frac{\partial\sigma_{ik}}{\partial x_k}\right)-F_{D_i}, \qquad (1)$$

where F_{D_i} are the components of the dynamic viscous drag force vector $\mathbf{F}_D$, which the skeleton exerts on the fluid per unit volume. The viscous drag force is a linear function of the solid strains and fluid displacements, given in the frequency domain in matrix form in terms of the relative motion between the two phases

$$\{\mathbf{F}_D\} = [\bar{Z}]\{\dot{\mathbf{u}}-\dot{\mathbf{U}}\}, \qquad (2)$$

where $[\bar{Z}]$ is the spatially-averaged dynamic viscous drag force impedance matrix per unit volume [5], for a transversely isotropic fibrous material

$$[\bar{Z}] = \frac{\phi}{A}\begin{bmatrix} J & 0 & 0 \\ 0 & J & 0 \\ 0 & 0 & K \end{bmatrix}. \qquad (3)$$

The coefficients J, K, are defined in terms of the analytical axial and transverse viscous drag force impedances for an individual fibre

$$Z_l = 2\pi a k_\beta \mu_f \frac{H_1^{(2)}(k_\beta a)}{H_0^{(2)}(k_\beta a)}, \qquad (4)$$

$$Z_t = j\pi\rho_f\omega a^2\left[1-\frac{4H_1^{(2)}(k_\beta a)}{k_\beta a H_0^{(2)}(k_\beta a)}\right], \qquad (5)$$

and where the shear wavenumber of the infinite viscous fluid is $k_\beta = \left(-j\omega\rho_f/\mu_f\right)^{1/2}$. Note that the dynamic viscous drag force impedance matrix may be defined for isotropic, and fully anisotropic materials as well as for a distribution of fibre diameters and orientation angles.

In a similar way, a momentum balance on the fluid phase of the porous material allows the equation of

motion of the fluid (fluid momentum equation) to be defined as

$$\left(1-\phi\right)\rho_f \ddot{U}_i = \frac{\partial \sigma}{\partial x_i} + F_{D_i} \ . \qquad (6)$$

Non-Equilibrium Fluid Dilatation

Under equilibrium conditions, stress and strain for any porous material are related by coupled constitutive stress-strain relations of the form

$$\{\sigma\} = [D]\{\varepsilon\} . \qquad (7)$$

When waves propagate in the porous fibrous material, assumed one-way heat transfer between the solid fibres and surrounding viscous fluid allows a thermal expansion of the fluid phase. This leads to an extension of the fluid dilatation terms away from equilibrium. Making use of the linearised entropy relations for a two-phase porous material, we can derive a new fluid dilatation expression [1], which is valid for non-equilibrium conditions

$$\chi\sigma = R\varepsilon + \left(Me_{xx} + Me_{yy} + Qe_{zz} \right) . \qquad (8)$$

Here, the fluid pressure term is now scaled by the frequency-dependent coefficient χ

$$\chi = \left[1 - \frac{\alpha\eta R}{j\omega\rho_f Cp_f \left(1-\phi\right)} \right] , \qquad (9)$$

where

$$\alpha = \eta T_f' \left\{ \frac{\rho_f Cp_f \left(1-\phi\right)}{\overline{Y}_e} + \frac{1}{j\omega} \right\}^{-1} , \qquad (10)$$

and $\overline{Y}_e$ is the effective thermal impedance function,

$$\overline{Y}_e = \frac{\phi}{A} \left[\frac{1}{Y_f} + \frac{1}{Y_s} \right]^{-1} , \qquad (11)$$

which is derived from the oscillatory thermal fields of the respective fluid and solid phases [6].

Transfer Matrix Acoustic Simulations

The complete description of coupled acoustic and structural wave propagation through the three-dimensional porous material is then provided by Eqs. (1, 6 and 8), where the viscous dissipation and thermal heat transfer behaviour has been defined in terms of microstructure-based analytical expressions. It is then straightforward to define a set of wave equations, and formulate a transfer matrix (TM) representation of the model [1, 4].

For validation purposes, we then consider plane acoustic wave propagation through a rigidly-backed finite thickness of the fibrous material, i.e. the standard acoustic impedance tube experiment. We have then used the material mean fibre diameter of 1.28 micrometres, and a fibre inclination angle of 50 degrees (from the *xy* plane) in the TM formulation to simulate the acoustic absorption behavior of a 50 *mm* thickness of material sample and compared this to measurements, as shown in Fig. (3).

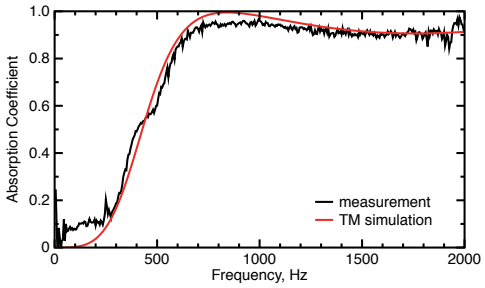

Figure 3. Measured and simulated normal-incidence absorption coefficient.

A very good agreement exists in the comparison between the numerical simulation and measured absorption coefficient across the entire frequency range. Material inertial and dissipative effects have been correctly represented in the simulation.

The list of material properties used for the TM simulation are provided in [1], and they consist of only the geometrical microstructure parameters, the constitutive properties for air and glass at 20 deg. C., and the measured macroscopic elastic properties of the material. We will also present results for this material using an expanded set of fibre diameter distributions and orientation angles in future work.

In addition, the analytical expressions for dynamic viscous drag impedance through the thickness of the material sample, as defined by Eq. (3), may also be scaled according to fibre diameter distributions and orientations to provide an estimate of the airflow resistance of the material (note that viscous drag force impedance and airflow resistivity have the same units). This is shown in Fig. (4), in the form of the low frequency (quasi-static) asymptote of the dissipative (real part) of $\overline{Z}_z$.

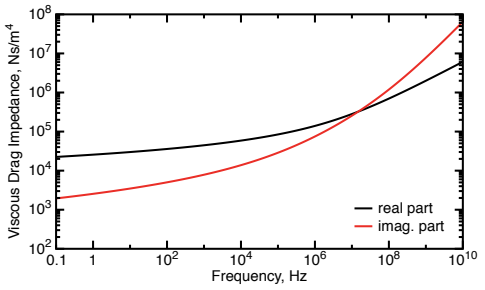

Figure 4. Dynamic viscous drag force impedance function.

The through-thickness measured value of airflow resistivity for this material was 23400 Ns/m^4, while the low frequency estimate provided by Eq. (3) was

22470 Ns/m^4, which was again in very good agreement.

Thermoviscous Acoustic Fluid Finite Element Modelling

In the formulation of the coupled equations for acoustic-structural wave propagation through a fibrous porous material presented here, where the viscous and thermal dissipation mechanisms have been derived entirely from microstructural considerations, the underlying assumption is that the dynamic viscous and thermal fields surrounding individual fibres do not interact significantly with the fields of neighbouring fibres. In the worst case, low frequency estimate, acoustic boundary layer theory [7] states that the viscous and thermal boundary layer penetration depths, for air at 20 deg. C and at 1 Hz, will be approximately l_{vor} = 2.2 mm and l_{th} = 2.6 mm, which is clearly beyond the average fibre spacing of 18.052 micrometres existing within the material.

Taken at face value, this would theoretically invalidate the assumptions inherent to the analytically derived viscous and thermal expressions in our formulation.

To address this, we have utilized the thermoviscous acoustic fluid modelling capabilities in COMSOL as a *virtual laboratory*, in order to fully understand the behaviour of the viscous and thermal boundary layers on the surface of the fibres, and also to reasonably assess the interaction of the boundary layers within a representative statistical array of fibres. In this approach, the fluid surrounding the solid glass fibres is then represented as a superposition of coupled acoustic, vorticity and entropy modal fields [7].

Single Fibre Boundary Layers

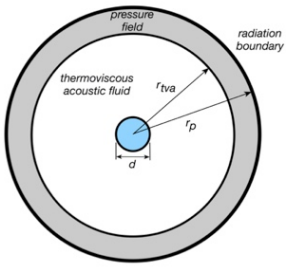

Figure 5. 2D oscillating cylindrical glass fibre embedded within a non-reflecting thermoviscous acoustic fluid.

The first case of a sinusoidally oscillating elastic cylinder, embedded in a non-reflecting infinite thermoviscous acoustic fluid was considered in order to establish a validation case for the FE numerical procedure. As a reference, the analytical relation for transverse dynamic drag force impedance, Eq. (5) was used.

The fluid region surrounding the fibre of mean diameter 1.28 micrometres was divided into two separate domains, an inner thermoviscous acoustic fluid one having a radius of 15 mm, which was then encased by a 5 mm thickness acoustic pressure field having a non-reflecting radiation boundary on the outer surface, as shown in Fig. (5). The excitation frequency was 1 Hz, and the fibre oscillation amplitude was chosen to be 0.01 micrometres in order to ensure linearity.

For this single fibre model, a combination of linear pressure, and quartic velocity and thermal elements were used for the thermoviscous fluid and acoustic pressure regions, respectively. Quartic elastic stress elements were used for the stress field internal to the fibre, which was then coupled to the surrounding thermoviscous fluid region. The simplicity of axisymmetric conditions was not considered for the analysis, since the modelling approach would be later scaled up towards a rectangular grid of random fibre diameters, specified according to the known statistical fibre diameter distribution. The combined single-fibre model described here contained a total of approximately 12 million degrees-of-freedom (DOF). Extreme care was taken to ensure that the decaying waves radiating outwardly through the thermoviscous acoustic fluid from the fibre surface have not experienced any unwanted boundary reflections.

Integrating over the fibre surface to estimate the traction forces, then allows the transverse dynamic viscous drag impedance per unit length values to be estimated. From the single fibre FE model. A value of 87642 Ns/m^4 was found, which is within 0.02 percent of the analytical result of 87665 Ns/m^4 as predicted by Eq. (5). With respect to the numerical difficulties present when trying to model such microscopic geometries with non-reflecting propagating waves using finite elements, these results should then be considered as a very satisfactory validation of the numerical FE modelling procedure.

The internal stress field within the cylindrical glass fibre has also been considered in the model. As expected, it was found that in this case, the large difference in bulk modulus between the surrounding thermoviscous fluid and solid glass fibre has led to negligible stress coupling between the two mediums.

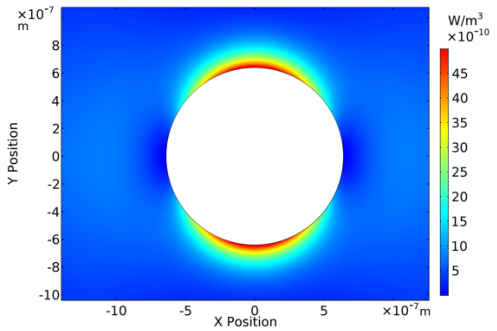

Figure 6. Viscous dissipation density on the fibre surface.

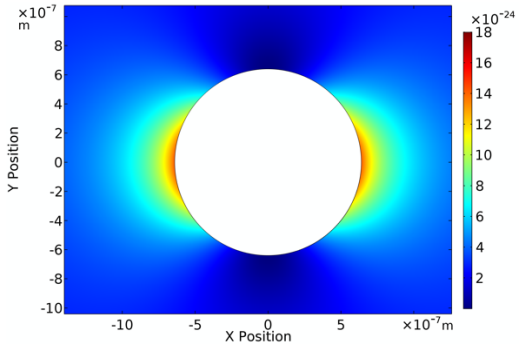

Figure 7. Thermal dissipation density on the fibre surface.

Examination of the viscous and thermal power dissipation density fields, as shown in Figs. (6, 7), indicates the concentration of the viscous and thermal boundary layer intensity in the immediate vicinity of the fibre surface, at micro and nano-scale levels. Considering these fields radially in the *x* direction from the fibre surface, as shown in Figs. (8, 9), further demonstrates that even for the very low excitation frequency of 1 Hz considered here, there is a concentration of the boundary layers to the immediate vicinity of the fibre surface. Furthermore, the viscous boundary layer, which is responsible for most of the dissipation losses in the analytical model, has decayed approximately 98 percent at the position of the next neighbouring fibre, according to the known fibre spacing of 18.052 micrometres. This is significantly different than the 2.2 mm viscous penetration depth value at 1 Hz.

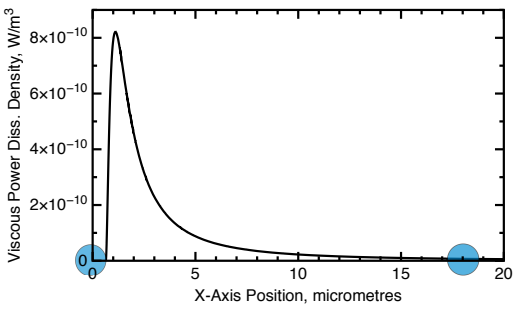

Figure 8. Viscous dissipation in the x-dir. from the fibre surface.

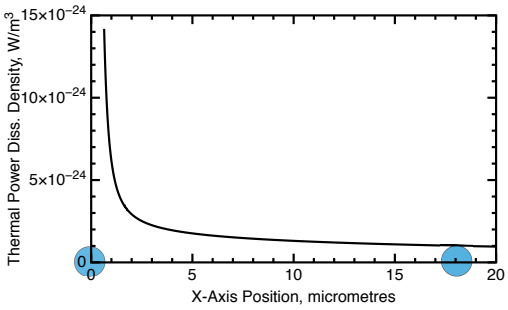

Figure 9. Thermal dissipation in the x-dir. from the fibre surface.

Further examination of the viscous and thermal dissipation densities also highlights that the dissipative potential of the thermal boundary layer is orders of magnitude less than the dissipation of the viscous boundary layer. This corresponds with our poroelastic equation formulations, where dissipation in the model is represented in terms of viscous fluid drag forces, and structural damping losses within the solid fibre skeleton. Heat transfer in the model is then primarily responsible for a thermal expansion of the fluid only.

The viscous boundary layer strength will increase with a reduction in fibre diameter, and will subsequently decrease with increasing fibre diameter, as shown in Fig. (10).

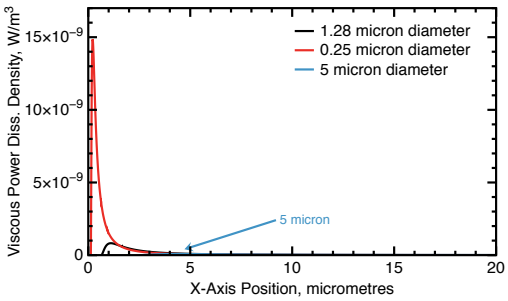

Figure 10. Viscous dissipation density for the diameter distribution range.

Here, the smallest, mean and largest fibre diameters from the statistical distribution are presented. The viscous dissipation potential of the nano-scale fibre geometries is shown to be significant, which would also apply to other classes of porous materials as well, such as foams with very fine strut diameters.

Representative Multi-Diameter Fibre Array

In order to investigate the significance of viscous and thermal boundary layer interaction between fibres, a more realistic case with a large distribution of fibre diameters was modelled. For this purpose, a model of an array of 225 fibres, uniformly distributed according to their diameter distribution, using the mean fibre spacing of 18.052 micrometers, was considered as schematically

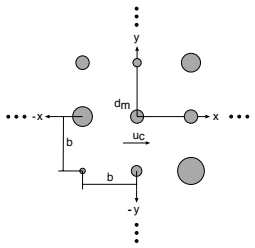

Figure 11. 225 fibre array, with 18.052 micrometre spacing and respecting the diameter distribution.

shown in Fig. (11). This model adds not only increased complexity due to a larger number of interacting fibres, it also incorporates the effects related to a variation of the fibre diameters in the array, for which the measured statistical distribution of diameters presented in [5] was incorporated. Using the verified single-fibre modelling procedure, the resulting FE model consisted of approximately 35 million degrees-of-freedom, based on a refined modelling criteria as compared to the single fibre case.

All fibres in the array were excited in-phase at a frequency of 1 Hz, and the fibre oscillation amplitude was chosen to be 0.01 micrometres in order to ensure linearity. This would correspond to a uniform rigid body motion of the entire material sample. The resulting viscous and thermal power dissipation density fields are shown in Figs. (12 and 13) respectively.

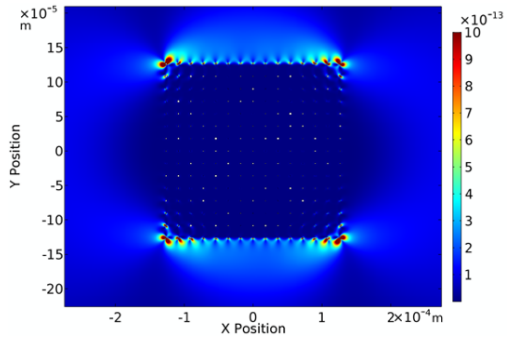

Figure 12. 225 fibre array viscous dissipation density.

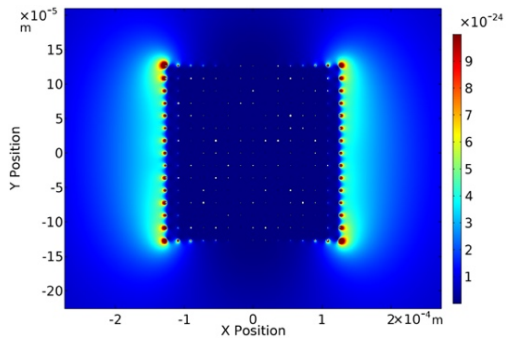

Figure 13. 225 fibre array thermal dissipation density.

As a comparison, the arithmetic mean of the viscous drag force impedance function, as calculated using the analytical expressions proposed here, and using the same measured statistical distribution of fibre diameters, gives a value of 79527 Ns/m^4. Integrating over the surfaces of all 225 fibres in the FE simulation, the arithmetic mean of the fibre reaction forces allowed the dynamic drag force impedance to be estimated as 78403 Ns/m^4, which is accurate to approximately 1.1 percent. This was deemed to be sufficient, and allows us to reliably draw conclusions about the interaction of the viscous and thermal boundary layers within the fibre array.

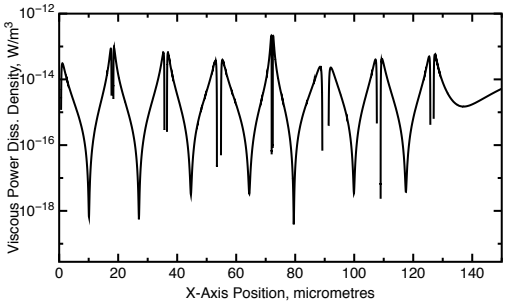

Figure 14. Viscous dissipation density in the x-dir. across the 225 fibre array. The origin is the central mean fibre diameter.

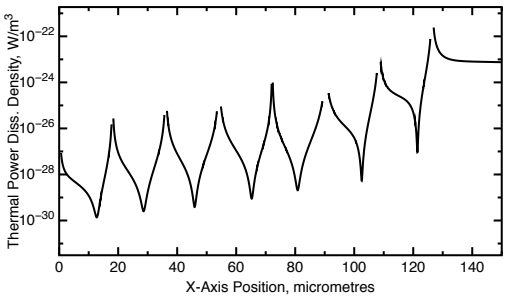

Figure 15. Thermal dissipation density in the x-dir. across the 225 fibre array. The origin is the central mean fibre diameter.

Considering these fields radially in the *x* direction from the central mean fibre diameter, as shown in Figs. (14 and 15), demonstrates that the viscous boundary layers maintain a uniqueness in amplitude around individual fibres as one moves across the fibre array. This suggests that for the known fibre spacing (18.052 micrometres) of the glass fibre insulation material considered, there is not a high level of boundary layer interaction to significantly impact the assumptions in the analytical model. This is also confirmed in the viscous drag force estimate comparison, where there is a very close comparison to the analytical solution, which is inherently based on the assumption of no field interaction between neighbouring fibres.

The thermal boundary layers trend upwards in amplitude with each subsequent fibre, indicating a certain level of interaction between the fibres. The reason for this is the build-up of a thermal wavefront

along the fibres at the outer boundary of the array. The significance of this will be investigated further in future work.

Conclusions

In our recent work, we have developed a new set of dynamic equations of motion for elastic-framed, transversely isotropic, lightweight, highly-porous fibrous insulation materials based entirely on physical microstructure considerations. Viscous losses are included in the model through analytical expressions for the dynamic drag impedance of cylindrical fibres, in a form similar to Biot's permeability tensor. Non-equilibrium conditions are included in the fluid dilatation expressions to characterise heat transfer effects between the fibre skeleton and surrounding fluid. Fibre spacing (i.e. porosity), and distributions of diameter and fibre orientation angles are considered as the microstructural parameters. A transversely isotropic transfer matrix representation of the model has been developed, with the subsequent acoustic simulation of an impedance tube experiment providing very good agreement with measurements.

The use of the Thermoviscous Acoustic Fluid modelling capabilities of COMSOL as a virtual laboratory tool, has proved invaluable in supporting these developments.

The underlying assumptions of the model are such that the dynamic viscous and thermal boundary layers on the surfaces of the distributions of neighbouring cylindrical fibre orientations and diameters do not interact. Using the analytical dynamic viscous drag force expression for transverse fibre oscillations as a reference, we have validated an accurate COMSOL finite element modelling procedure to simulate the boundary layers on the surface of a single fibre. This approach was then scaled up to accurately model a random fibre array representative of the actual material diameter distribution.

These modelling efforts have provided great insight into the controlling dissipation mechanisms within the fibrous insulation material, and has demonstrated that the assumption regarding no significant interaction of viscous shear and thermal boundaries between neighbouring fibres is valid for the high porosity glass fibre insulation investigated in this work.

Our future work will now include a microstructural representation of the transversely isotropic elastic properties of the material.

References

1. Semeniuk, B.P., Göransson, P. and Dazel, O., "Microstructure based modelling of the thermal and viscous dissipation of a transversely isotropic porous fibrous insulation material," *Proceedings of ISMA2018 - International Conference on Noise and Vibration Engineering*, Leuven, Belgium, September 17-19, 2018.
2. He, M., Perrot, C., Guilleminot, J., Leroy, P. and Jacqus, P., "Multiscale prediction of the acoustical properties of glass wools: Computational study and experimental validation," *The Journal of the Acoustical Society of America*, **Vol. 143, No. 6**, pp. 3283-3299, 2018.
3. Xue, Y., Bolton, J.S., Gerdes, R., Lee, S. and Herdtle, T., "Prediction of airflow resistivity of fibrous acoustical media having two fiber components and a distribution of fiber radii," *Applied Acoustics,* **Vol. 134**, pp. 145-153, 2018.
4. Allard, J.F. and Atalla, N., *Propagation of Sound in Porous Media: Modelling Sound Absorbing Materials*, John Wiley & Sons, 2nd ed., 2009.
5. Semeniuk, B.P. and Göransson, P., "Microstructure based estimation of the dynamic drag impedance of lightweight fibrous materials," *The Journal of the Acoustical Society of America*, **Vol. 141, No. 3**, pp. 1360-1370, 2017.
6. Kuntz, H.L. and Perreira, N.D., "Oscillatory conductive heat transfer for a fiber in an ideal gas," *Journal of Heat Transfer*, **Vol. 107, No. 1**, pp. 52-56, 1985.
7. Pierce, A., *Acoustics: An Introduction to Its Physical Principles and Applications*, Acoustical Society of America, 1989.
5. "COMSOL Multiphysics v. 5.3a www.comsol.com COMSOL AB, Stockholm, Sweden."

Acknowledgements

The second author gratefully acknowledges the funding from the Swedish Research Council, grant nr 2015-04258, which has partially contributed to this work.